Efficient Optically-Pumped Semiconductor Optical Amplifier in a Coupled-Waveguide Configuration: A Novel Proposal

Nithin Vogirala, M. R. Shenoy, and Yogesh Kumar

***Abstract*—We propose an efficient scheme of optical pumping and a compact design of an optically-pumped semiconductor optical amplifier (OP-SOA), with gain characteristics which are qualitatively similar to that of conventional (electrically-pumped) SOA. The optical pump is coupled into the 'active waveguide' from an adjacent channel waveguide, called 'pump waveguide'; by suitably tailoring the coupling between the two waveguides, selective transfer of pump power all along the active waveguide can be achieved. We show that optical pumping through the coupled-waveguide configuration is efficient over the existing schemes of optical pumping in semiconductors. The optical pump can be coupled into the pump waveguide through a separate fiber-pigtail, just as the signal is coupled to the active waveguide in commercially available SOA. Thus, the OP-SOA would be a stand-alone 3-port integrated optical device, without any electrical connections. The proposed scheme enables optical-to-optical gain control, in place of the current-controlled gain in conventional SOA. Performance characteristics of the OP-SOA are simulated for an InGaAsP/InP heterostructure device using a well-established model. It is found that for an input optical pump power of 25 dBm at the wavelength of 1310 nm, a small signal gain $>$30 dB is achieved at the wavelength of 1550 nm.**

***Index Terms*—Optical pumping, semiconductor optical amplifiers, waveguide coupling.**

I. Introduction

SEMICONDUCTOR optical amplifiers (SOAs) are commonly used as gain medium in optical communication systems and networks. Due to the presence of strong optical nonlinearities, SOAs are also employed in various optical signal processing operations such as optical logic, wavelength conversion and optical switching [1]–[4]. The integration capability of the SOA makes it a key component in optical functional devices and photonic integrated circuits (PIC) [5], [6]. Conventionally, SOAs are biased by a current source through suitable electrode geometry to confine the current into the active region [5]–[7]. There is a growing need for optically-controlled photonic devices to enable an all-optical platform for signal processing [8]–[10]. Optical pumping of quantum dot SOA (QD-SOA) has been demonstrated [11]; however, it is fabricated using strained semiconductor heterostructures, and is difficult to integrate in practical photonic systems for field applications. Optical pumping in the form of 'assist-light injection' in conventional SOA for faster gain recovery has been demonstrated [12]–[15]. However, the 'end-pumping scheme' employed in this case is highly inefficient because most of the optical power gets absorbed within a short length from the input end due to the high absorption coefficient, and therefore, the latter portion of the active waveguide remains un-pumped [13]. Indeed, this has been the major drawback in realizing an optically-pumped SOA (OP-SOA) using the direct end-pumping configuration. Optical pumping through irradiation from outside is inefficient because only a small fraction of the pump power will be absorbed in the active medium (due to its small thickness $\sim$0.1 μm), and the remaining power will be unutilized [16].

In this paper, we propose a 3-port OP-SOA which shows qualitatively similar gain characteristics as that of a conventional SOA. In the proposed coupled-waveguide structure, the pump is transferred almost unidirectionally to the active waveguide, resulting in a compact and efficient scheme of optical pumping. In an earlier communication, we had reported the waveguide-coupled scheme for 'assist-light injection' to enhance the gain recovery in a conventional SOA [17]. The pumping scheme in [17] is based on buried channel coupled waveguide structure, with a large aspect ratio of active waveguide resulting in multiple transverse modes and high polarization dependence of the device, which is not desirable in many applications. In this paper, by an appropriate choice of waveguide materials, we also present an improved coupling scheme wherein only the pump couples between the pump waveguide and the active waveguide, whereas the signal does not couple between the waveguides. This gives the flexibility in designing the active waveguide with a near square cross section, resulting in a single-mode operation and low polarization dependence of the device. Further, the OP-SOA in the proposed scheme does not require doped semiconductors forming p-n junctions for carrier injection; this would also lead to lower scattering loss for carriers in the semiconductor medium. Thus, an efficient optical pumping scheme is proposed to realize an 'electrically-independent 3-port OP-SOA'. OP-SOAs that employ remote pumping through optical fibers may find applications in hazardous environment bereft of provision for electrical power.

Manuscript received September 13, 2021; revised October 10, 2021; accepted October 14, 2021. Date of publication October 19, 2021; date of current version November 3, 2021. *(Corresponding author: Nithin Vogirala.)*

Nithin Vogirala and M. R. Shenoy are with the Department of Physics, Indian Institute of Technology Delhi, Hauz Khas, New Delhi 110016, India (e-mail: v.nithin@physics.iitd.ac.in; mrshenoy@physics.iitd.ac.in).

Yogesh Kumar is with the Defense Research and Development Organization, New Delhi 110011, India (e-mail: yog_yogeshkumar@yahoo.com).

Digital Object Identifier 10.1109/JPHOT.2021.3120846

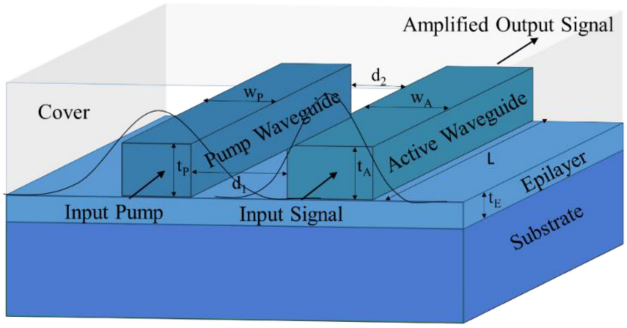

Fig. 1. Schematic of the proposed OP-SOA in which pumping of the active waveguide takes place through evanescent wave coupling in the ridge-waveguide coupler.

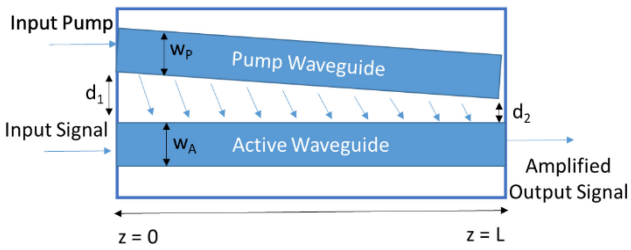

Fig. 2. Top-view of the proposed OP-SOA showing the design of the coupled-waveguide configuration; pump power is coupled into the pump waveguide at z = 0, and it is transferred to the active waveguide through evanescent wave coupling.

In the following, details of the proposed scheme along with performance characteristics of the OP-SOA are presented. Section II discusses the proposed scheme including the design of the coupled-waveguide configuration, and Section III deals with the choice of pump wavelength and the choice of materials. Coupling characteristics are discussed in Section IV. The numerical model for the simulation is outlined in Section V, and the steady-state performance characteristics of the proposed device are simulated in Section VI.

II. Scheme of Optical Pumping

Fig. 1 shows a schematic of the proposed device: A ridge-waveguide directional coupler comprising of the pump waveguide and the active waveguide, which can be fabricated on a semiconductor substrate. The pump is injected through the input facet of the pump-waveguide, which couples to the active waveguide through evanescent field interaction between the two waveguides, all along its length. The coupled pump power is absorbed throughout the active waveguide, and thus the carriers (electron-hole pairs) are generated all along the active waveguide. When the carrier density exceeds its threshold value, amplification of the signal takes place in the active waveguide, and the amplified output is obtained at the output facet of the active waveguide.

Fig. 2 shows the top view of the proposed device, indicating the design of the coupled-waveguide configuration. The dimensions of the pump and the active waveguide are chosen such

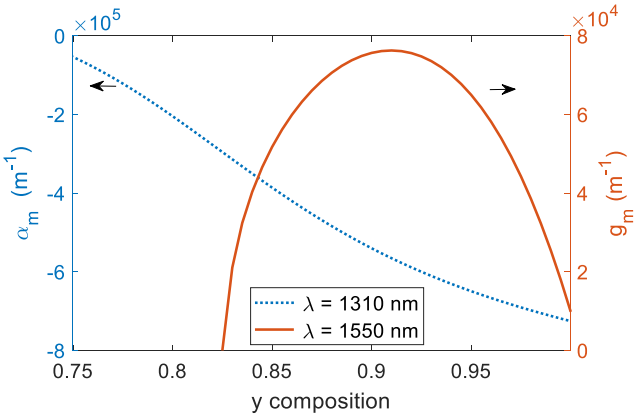

Fig. 3. Variation of the material absorption coefficient, α_{m} at 1310 nm (dotted line) and gain coefficient, gm at 1550 nm (solid line) with y composition of $In_{1-x}Ga_xAs_yP_{1-y}$ at the carrier density $N = 2 \times 10^{24}$ m^{-3}.

that they are single-moded at both the pump and the signal wavelengths, so that the input pump excitation and the coupling between the waveguides can be predicted and controlled accurately. The materials of the pump and active waveguides have different refractive indices, and the inter-waveguide separation varies linearly from d_1 (at z = 0) to d_2 (at z = L).

III. The Choice of Materials

We have designed the device such that the amplification occurs in the optical communication band around 1550 nm. The pump wavelength is chosen to be at 1310 nm because (i) the wavelength corresponds to a low-loss window of the optical fiber, which is important for remotely pumped amplifiers, (ii) the absorption coefficient of the active waveguide material is high around this wavelength, and (iii) the wide availability of high-power diode lasers at this wavelength. The proposed device is based on lattice-matched $In_{1-x}Ga_xAs_yP_{1-y}$/InP material system with x = 0.46y [18]. The substrate is InP on which there is an epilayer of $In_{1-x}Ga_xAs_yP_{1-y}$/InP. The pump and the active ridge waveguides are located in close proximity on the epilayer with different compositions (x, y) of $In_{1-x}Ga_xAs_yP_{1-y}$; a polycrystalline silicon overlay forms the top cover.

The material gain (or absorption) coefficient g_{m} (or α_{m}) in the $In_{1-x}Ga_xAs_yP_{1-y}$ active region depends on the carrier density N and the wavelength λ [18]:

$$g_m\ (N,\lambda) = \frac{\lambda^2}{4\sqrt{2}\,\pi^{\frac{3}{2}} n_1^2 \tau} \left(\frac{4\pi m_e m_{hh}}{h\,(m_e + m_{hh})}\right)^{\frac{3}{2}} * \sqrt{\frac{c}{\lambda} - \frac{E_g\,(N)}{h}}\,(f_c\,(\lambda) - f_v\,(\lambda)) \quad (1)$$

where τ is the radiative carrier recombination lifetime; m_e and m_{hh} are the effective masses of the electrons in the conduction band and the heavy holes in the valence band, respectively; E_g is the bandgap energy; f_c and f_v are the Fermi-Dirac distributions in the conduction band and the valence band, respectively, in quasi-equilibrium.

TABLE I
LIST OF THE WAVEGUIDE PARAMETERS USED IN THE DESIGN OF THE PROPOSED DEVICE

Parameter	Value
Length (L)	500 μm
Width of Active waveguide (w_A)	1 μm
Thickness of Active waveguide (t_A)	0.8 μm
Width of Pump waveguide (w_P)	1 μm
Thickness of Pump waveguide (t_P)	0.8 μm
Thickness of Epilayer (t_E)	4 μm
Inter-waveguide separation, d(z) (linearly decreasing with z)	1 μm (z = 0) 0.5 μm (z = L)

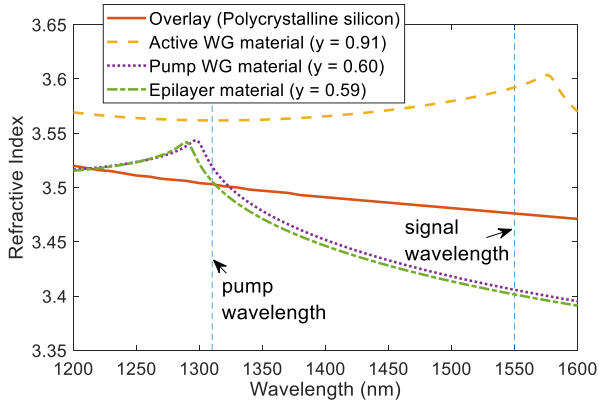

Fig. 4. Dispersion curves for the materials used in the epilayer, pump waveguide, active waveguide and the overlay.

Fig. 3 shows the variation of the material absorption coefficient at 1310 nm (dotted line) and the gain coefficient at 1550 nm (solid line) with the composition 'y' of $In_{1-x}Ga_xAs_yP_{1-y}$ respectively, at a carrier density N of 2×10^{24} m^{-3}. For the wavelength 1550 nm, the peak gain occurs at the material composition $y = 0.91$. At this composition of $In_{1-x}Ga_xAs_yP_{1-y}$, the absorption coefficient at 1310 nm is also very high ($\approx 5.6 \times 10^5$ m^{-1}). The band-edge wavelength (or cutoff wavelength) at this composition is 1577 nm. Thus, the composition of $In_{1-x}Ga_xAs_yP_{1-y}$ with $y = 0.91$ for the core of the active waveguide is very favorable for operation of the amplifier. The bandgap energy $E_g\,(x,y)$ of $In_{1-x}Ga_xAs_yP_{1-y}$ is given by [19]:

$$E_g(x,y) = \left(1.35 + 0.668x - 1.068y + 0.758x^2 + 0.078y^2 - 0.069xy - 0.332x^2y + 0.03xy^2\right) \quad (2)$$

The material composition of the core (guiding region) of the pump waveguide has to be chosen such that it is transparent at the pump wavelength, i.e., the band-edge wavelength should be less than the pump wavelength. Accordingly, we have chosen $y = 0.60$, which corresponds to a band-edge wavelength of 1297 nm. The composition of the epilayer is chosen such that the refractive indices at both pump and signal wavelengths are less than the corresponding refractive indices of the materials of the pump and the active waveguide. We have chosen $y = 0.59$, which corresponds to a band-edge wavelength of 1290 nm. The band-edge wavelength is chosen to be close to the pump wavelength to ensure that Δn (refractive index difference between core and cladding) is relatively small, and therefore the dimensions of the waveguide need not be too small to maintain the single-mode condition [7]. The list of the parameters used in the design is given in Table I.

Fig. 4 shows the material dispersion curves for the various materials chosen above in the design of the proposed device [19], [20]. It may be noted that at the pump wavelength (1310 nm), both the pump waveguide material (dotted line) and the active waveguide material (dashed line) serve as core materials (of higher refractive index), with epilayer and cover (overlay) acting as the surrounding clad materials (of lower refractive index). Therefore, at the pump wavelength, both the pump waveguide and the active waveguide support guided modes; however, at the signal wavelength (1550 nm), only the active waveguide supports guided modes, while the pump waveguide does not support any guided mode. This is because at 1550 nm, the refractive index of the cover (overlay) is larger than the refractive index of the pump waveguide material. Therefore, the signal in the active waveguide does not couple into the pump waveguide, and the amplified signal is obtained at the output end of the active waveguide. Moreover, from Fig. 4 it can be seen that at the pump wavelength (1310 nm), the refractive index of the epilayer and the overlay are almost equal; this implies that the waveguide is nearly symmetric, and therefore the fundamental mode of the pump waveguide at 1310 nm would have a near-circular cross section. Since the pump power is usually coupled into the pump waveguide through a fiber pigtail, the input pump coupling efficiency in this case can also be very high.

In the proposed design, the two coupled ridge waveguides have their core layers made up of slightly different compositions of the alloy $In_{1-x}Ga_xAs_yP_{1-y}$, and it would require selective lithographic procedure (including growth and etching) for the core layers of the ridge. This would necessiate two or three additional steps in the fabrication. All other layers comprise of the same material and thickness for both the waveguides. It may also be noted that the proposed device does not require the fabrication steps of metallization and provision of electrical contacts to power the device.

IV. COUPLING CHARACTERISTICS

We have used the OptiBPM software to simulate the coupling characteristics between the waveguides [21]. Fig. 5 shows the coupling characteristics at the pump wavelength, when the pump is injected at $z = 0$ in the pump waveguide. To illustrate the effect of absorption in the active waveguide on the coupling characteristics at this wavelength, we have taken two absorption coefficients i.e., $\alpha_1 = -5.65 \times 10^5$ m^{-1}, which is the actual absorption coefficient obtained for our design parameters, and $\alpha_2 = -5.65 \times 10^3$ m^{-1} (i.e., two orders less than α_1). As shown in the figure, for our chosen design parameters, the pump

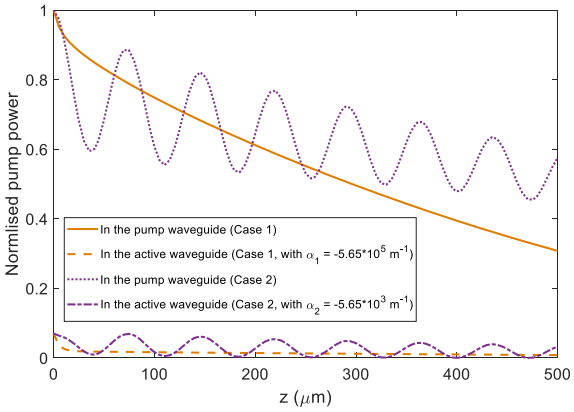

Fig. 5. Pump power profile in the active and the pump waveguides for two different absorption coefficients of the active waveguide material (α_1 and α_2) at the pump wavelength, when the pump is injected at z = 0; the pump waveguide is assumed to be non-absorbing.

is almost uni-directionally transferred all along the active waveguide with minimal back-coupling. However, for the case of lower absorption (α_2), the pump profile in the active waveguide is like a typical decaying sinusoidal oscillation, with a fraction of pump power back-coupling into the pump waveguide. The unidirectional nature of pump power transfer is because of the high absorption coefficient in the active waveguide. This compounds to the nature of coupling characteristics of the non-identical pump and active waveguides, i.e., a weak coupling from the active waveguide (which supports a strongly-confined guided mode) to the pump waveguide (which supports a weakly-confined guided mode) [17], [22]. This, in effect, results in a near-optimum design of the coupled-waveguide configuration to achieve efficient pumping of the active waveguide. At the output-end of the OP-SOA, about 30% of unabsorbed pump power still remains; it is possible to make it zero by suitably adjusting the coupling between the waveguides. However, this requires a longer length of the OP-SOA, and it would lead to a reduction in the overall gain and increase in the ASE noise.

V. Modelling of the OP-SOA

For simulation of carrier dynamics and performance characteristics of the OP-SOA, we have followed the Connelly's model, which includes the co-propagation of probe light (signal), the co-propagation of pump light, and the co- and counter-propagating amplified spontaneous emission (ASE). The active region of the SOA is divided into a suitable number of sections, each of length Δz. In Connelly's model, the carrier density N in the i^{th} section of the SOA at time t is evaluated through the following carrier density rate equation [18]:

$$\frac{dN_i(z,\ t)}{dt} = \frac{I}{edWL} - R - \frac{\Gamma}{dW}\left\{\frac{\lambda_S g_m(N_i,\lambda_S)}{hc}P_S(z,t)\right\} - \frac{2\Gamma}{dW} \left\{\sum_{j=0}^{N_m-1}\frac{\lambda_j g_m(N_i,\ \lambda_j)}{hc}K_j\left[P^+_{ASE}(N(z)) + P^-_{ASE}(N(z))\right]\right\} \tag{3}$$

where the symbols have their usual meaning. In a conventional SOA, only the first term in the RHS of (3) generates the carriers (due to bias current) and other terms deplete the carriers. For the optically-pumped SOA, we replace this term and modify the rate equation to account for the carrier generation due to the optical pump power, $P_P(z, t)$ coupled into the active waveguide:

$$\frac{dN_i(z,\ t)}{dt} = -\frac{\Gamma}{dW}\left\{\frac{\lambda_P g_p(N_i,\lambda_P)}{hc}P_P(z,t)\right\} - R - \frac{\Gamma}{dW}\left\{\frac{\lambda_S g_m(N_i,\lambda_S)}{hc}P_S(z,t)\right\} - \frac{2\Gamma}{dW} * \left\{\sum_{j=0}^{N_m-1}\frac{\lambda_j g_m(N_i,\ \lambda_j)}{hc}K_j\left[P^+_{ASE}(N(z)) + P^-_{ASE}(N(z))\right]\right\} \tag{4}$$

Since the pump wavelength corresponds to the absorption region of the active waveguide, g_p in (4) is negative (see Fig. 3); thus, the first term generates carriers, leading to the optical pumping operation of the SOA.

The confinement factor for the TE and the TM modes differs slightly by ~5% due to the near square cross section of the active waveguide (1 μm x 0.8 μm) [5], and for simplicity, the confinement factor is assumed to be the same for both TE and TM polarizations by several earlier research work [13], [18]. Therefore, in our analysis, we have considered the OP-SOA as a polarization independent device.

The evolution of the signal in the active waveguide of the OP-SOA (assuming no signal power coupling from the active waveguide to the pump waveguide), is given by the travelling wave equation [18]:

$$\frac{dP_S(z)}{dz} = (\Gamma g_m(N,\ \lambda_S) - \alpha)\ P_S(z) \tag{5}$$

The pump power (P_P) in each section of the active waveguide comprises of the propagating pump power from the previous section plus the power coupled from the pump waveguide into that section. To estimate the pump power in any particular section of the active waveguide ($P_P{}^{AW}(z)$) due to the propagating pump from the previous section, we use the travelling wave equation [17]:

$$\frac{dP_P^{AW}(z)}{dz} = (\Gamma g_m(N,\ \lambda_P)\ - \alpha)\ P_P^{AW}(z) \tag{6}$$

We then add the pump power coupled from the pump waveguide ($P_P{}^{CW}(i)$) into that section, to obtain the net pump power in the particular section of the active waveguide:

$$P_P\ (z + \Delta z) = P_P^{AW}(z) + P_P^{CW}(i) \tag{7}$$

Here $P_P{}^{CW}(i)$ refers to the pump power added to the i^{th} segment of SOA, which is determined by using the OptiBPM software. Equations (1) and (4)-(7) are employed to simulate the performance characteristics of the OP-SOA. Other relevant parameters are as listed in [18].

VI. Results and Discussion

In this section, we present the simulation results on the performance characteristics of an InGaAsP/InP OP-SOA, pumped

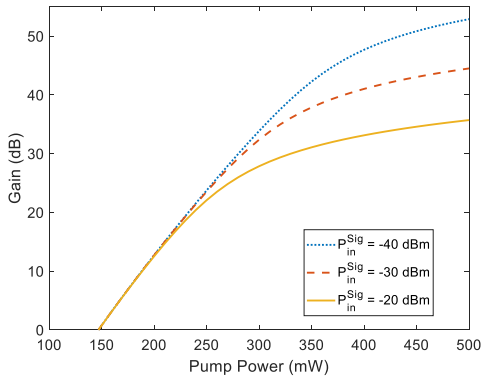

Fig. 6. Gain variation with input pump power in the 3-port OP-SOA for different input signal powers (P_{in}).

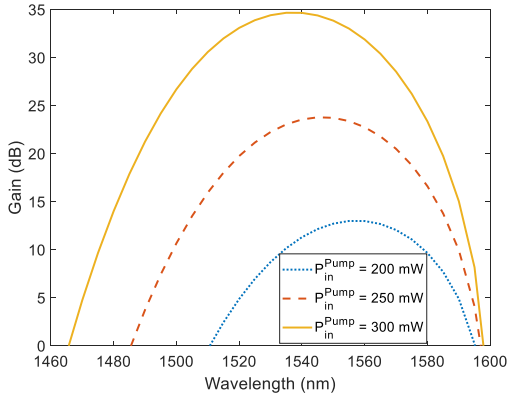

Fig. 7. Gain spectra of the 3-port OP-SOA for three different pump powers (P_{pump}) for input signal power of -40 dBm.

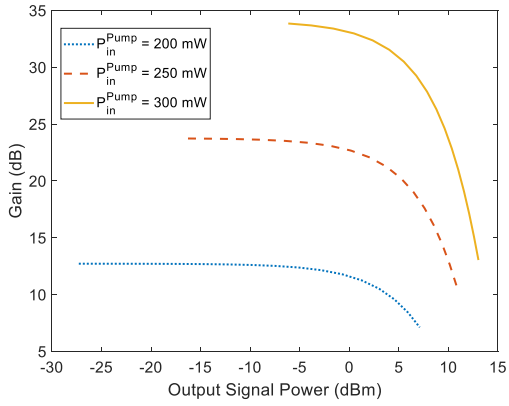

Fig. 8. Output saturation characteristics of the 3-port OP-SOA for three different pump powers (P_{pump}).

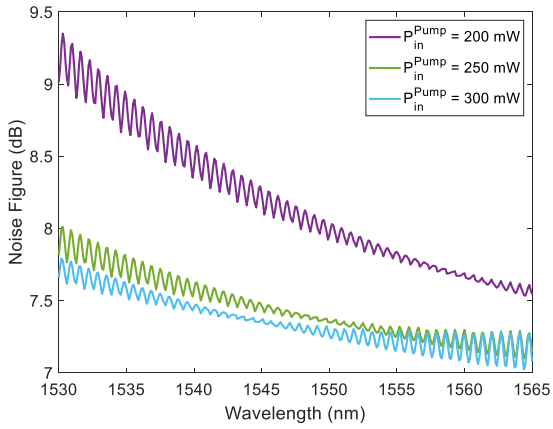

Fig. 9. Noise figure spectrum of the 3-port OP-SOA for three different pump powers (P_{pump}).

by an optical source at 1310 nm wavelength. Fig. 6 shows the gain variation with pump power for three different input signal powers. The threshold pump power for onset of signal gain is 148 mW, and it remains the same for different input signal powers. The threshold pump power in the OP-SOA is a characteristic parameter equivalent to the 'transparency current' in a conventional SOA. For an input signal power of -40 dBm at 1550nm, with 250 mW of pump power, the gain ≈ 25 dB. For higher pump powers the gain approaches saturation, as expected. To compare the efficiency of the proposed design of the OP-SOA with an OP-SOA employing the end-pumping scheme, in which the pump is directly coupled into the active-waveguide along with the signal (end-pumping), we also carried out simulations for the latter scheme. For an input signal power of -40 dBm at 1550nm, with 250 mW of pump power, there was a net signal loss of ≈ 6 dB. When the pump is directly injected into the active waveguide, only the initial part ($\approx$100 μm) of the active waveguide is pumped, whereas latter part is largely unpumped. Therefore, the carriers that amplify the signal are only generated at the initial portion; at the latter portion, the amplified signal undergoes absorption, leading to a net loss. This shows that the proposed pump coupling scheme is more efficient than the end-pumping scheme.

Fig. 7 shows the simulated gain spectrum of the OP-SOA for three different values of the optical pump power (P_{pump}). As the pump power increases, the density of carriers generated also increases. These generated carriers (electrons) occupy relatively higher energy levels in the conduction band, and a re-distribution of the carrier density profile. This leads to a gain spectrum with higher peak gain and an increase in the bandwidth as well as a shift in the peak gain toward higher energy, or lower wavelength.

Fig. 8 shows the amplifier saturation characteristics for three different pump powers. The output saturation power increases with increase in the optical pump power. All the simulated gain characteristics are qualitatively similar to the gain characteristics of a conventional SOA with different bias currents. The saturation characteristics are also similar to those of an erbium doped fiber amplifier (EDFA) for different pump powers [23].

The noise figure (*NF*) of the OP-SOA is given by [18]:

$$NF = 10\log_{10}\left(\frac{\sigma_{ASE}(\nu)}{h\nu G(\nu)} + \frac{\eta_{out}}{G(\nu)}\right) \tag{8}$$

where $\sigma_{ASE}(\nu)$ and $G(\nu)$ are the spontaneous emission noise power spectral density at the output and the fiber-to-fiber gain at the frequency ν, respectively; η_{out} is the output coupling

efficiency. Following the numerical model outlined in [18], we have calculated $\sigma_{ASE}(\nu)$ and $G(\nu)$ at the resonant and anti-resonant frequencies using the rate equations. The obtained values are used to calculate the noise figure in Equation (8). It can be seen from Fig. 9 that as the pump power increases, the noise figure decreases. This is because higher the gain, lower is the noise figure. The zig-zag pattern is due to the presence of resonant frequencies (dip) and anti-resonant frequencies (peak) within the amplifier bandwidth [18]. The oscillations arise due to the finite reflectivity of the facets of the active waveguide. Although the facets of an SOA are anti-reflection coated, there is some residual reflectivity. The reflectivity used for each facet is 5×10^{-5} [18].

VII. Conclusion

We have proposed a novel device configuration to realize efficient optically-pumped semiconductor optical amplifier through transverse waveguide-coupling of the pump. The proposed device conveniently permits tailoring of the carrier density distribution along the active region. Numerical results show that the OP-SOA exhibits gain and saturation characteristics that are qualitatively similar to those of the conventional SOA. Optical pumping provides the desirable optical-to-optical gain control and could have potential applications in all-optical signal processing. The proposed device could be a stand-alone three port integrated optical device, without any electrical connections, and it could form a new platform for OP-SOA based devices.

References

[1] J.-Y. Kim, J.-M. Kang, T.-Y. Kim, and S.-K. Han, "All-optical multiple logic gates with XOR, NOR, OR, and NAND functions using parallel SOA-MZI structures: Theory and experiment," *J. Lightw. Technol.,* vol. 24, no. 9, pp. 3392–3399, Sep. 2006.

[2] H. N. Tan, M. Matsuura, and N. Kishi, "Enhancement of input power dynamic range for multiwavelength amplification and optical signal processing in a semiconductor optical amplifier using holding beam effect," *J. Lightw. Technol.,* vol. 28, no. 17, pp. 2593–2602, Sep. 2010.

[3] A. Sobhanan, L. N. Venkatasubramani, R. D. Koilpillai, and D. Venkitesh, "Dispersion and nonlinearity distortion compensation of the QPSK/16QAM signals using optical phase conjugation in nonlinear SOAs," *IEEE Photon. J.*, vol. 12, no. 1, Feb. 2020, Art. no. 7800107.

[4] Z. G. Lu, P. Bock, J. R. Liu, M. Florjanczyk, and T. Hall, "Ultrabroad tunable wavelength conversion in a semiconductor optical amplifier," *Microw. Opt. Technol. Lett.*, vol. 48, no. 11, pp. 2139–2142, 2006.

[5] N. K. Dutta and Q. Wang, *Semiconductor Optical Amplifiers*, 2nd ed., Toh Tuck Link, Singapore: World Scientific, 2006.

[6] Infinera, "The advantages of indium phosphide photonic integration in high-performance coherent optics," Oct. 21, 2019. [Online]. Available: https://www.infinera.com/white-paper/The-Advantages-of-Indium-Phosphide-Photonic-Integration-in-High-performance-Coherent-Optics

[7] G. P. Agrawal, *Fiber-Optic Communication Systems*, 4th ed. Hoboken, NJ, USA: Wiley, 2010.

[8] A. E. Willner, S. Khaleghi, M. R. Chitgarha, and O. F. Yilmaz, "All-optical signal processing," *J. Lightw. Technol.,* vol. 32, no. 4, pp. 660–680, Feb. 2014.

[9] Y. Jiang, X. Luo, L. Hu, J. Wen, and Y. Li, "All optical add-drop multiplexer by utilizing a single semiconductor optical amplifier," *Microw. Opt. Technol. Lett.,* vol. 52, no. 9, pp. 1977–1980, Jul. 2010.

[10] X. Zhang, C. Zhao, H. Liu, D. Liu, and D. Huang, "20 Gb/s all-optical and gates and nor gates using cascaded SOAs," *Microw. Opt. Technol. Lett.,* vol. 49, no. 2, pp. 484–487, Dec. 2007.

[11] D. Bimberg and U. W. Pohl, "Quantum dots: Promises and accomplishments," *Mater. Today*, vol. 14, no. 9, pp. 388–397, Sep. 2011.

[12] M. Amaya, A. Sharaiha, and F. Ginovart, "Comparison between co- and counter-propagative optical injection near the transparency wavelength on SOA static and dynamic performances," *Opt. Commun.,* vol. 246, no. 1, pp. 67–71, Feb. 2005.

[13] H. Wang, J. Wu, and J. Lin, "Studies on the material transparent light in semiconductor optical amplifiers," *J. Optic. Pure Appl. Optic.,* vol. 7, no. 9, pp. 479–492, Aug. 2005.

[14] E. Zhou, X. Zhang, and D. Huang, "Evaluating characteristics of semiconductor optical amplifiers using optical pumping near the transparency," *J. Opt. Soc. Amer. B,* vol. 24, no. 10, pp. 2647–2657, Oct. 2007.

[15] F. Ginovart, M. Amaya, and A. Sharaiha, "Semiconductor optical amplifier studies under optical injection at the transparency wavelength in copropagative configuration," *J. Lightw. Technol.,* vol. 25, no. 3, pp. 840–849, Mar. 2007.

[16] Y. Kumar and M. R. Shenoy, "A novel scheme of optical injection for fast gain recovery in semiconductor optical amplifier," *IEEE Photon. Technol. Lett.,* vol. 26, no. 9, pp. 933–936, May 2014.

[17] V. Nithin, Y. Kumar, and M. R. Shenoy, "Novel scheme of assist-light injection through waveguide coupling in a semiconductor optical amplifier for fast gain recovery," *Opt. Commun.,* vol. 359, pp. 419–425, Jan. 2016.

[18] M. J. Connelly, "Wideband semiconductor optical amplifier steady-state numerical model," *IEEE J. Quantum Electron.,* vol. 37, no. 3, pp. 439–447, Mar. 2001.

[19] S. Seifert and P. Runge, "Revised refractive index and absorption of In1-xGaxAsyP1-y lattice-matched to InP in transparent and absorption IR-region," *Opt. Mater. Exp.,* vol. 6, no. 2, pp. 629–639, Feb. 2016.

[20] M. A. Green and M. J. Keevers, "Optical properties of intrinsic silicon at 300 K," *Prog. Photovolt.,* vol. 3, pp. 189–192, Jan. 1995.

[21] A. Kumar, S. Kumar, and S. K. Raghuwanshi, "Implementation of XOR/XNOR and AND logic gates by using Mach–Zehnder interferometers," *Optik,* vol. 125, no. 19, pp. 5764–5767, Oct. 2014.

[22] A. Hardy and W. Streifer, "Coupled mode theory of parallel waveguides," *J. Lightw. Technol.,* vol. 3, no. 5, pp. 1135–1146, Oct. 1985.

[23] E. Desurvire, *Erbium-Doped Fiber Amplifiers: Principles and Applications*, 1st ed., New York, NY, USA: Wiley, 2002.